Enhanced Oxygen Evolution at Hydrous Oxy-Hydroxide Modified Iron Electrodes in Aqueous Alkaline Solution.

Michael E.G. Lyons[*] *and Richard L Doyle*

Physical and Materials Electrochemistry Laboratory, School of Chemistry, University of Dublin, Trinity College, Dublin 2, Ireland.
[*]E-mail: melyons@tcd.ie

Outstanding issues regarding the film formation and the oxygen evolution reaction (OER) electrocatalytic behaviour of multicycled iron oxyhydroxide films in aqueous alkaline solution have been revisited. The oxide is grown using a repetitive poltential multicycling technique, and the mechanism of the latter hydrous oxide formation process has been discussed. A duplex layer model of the oxide/solution interphase region is proposed. The acid/base behaviour of the hydrous oxide and the microdispersed nature of the latter material has been emphasised. The hydrous oxide is considered as a porous assembly of interlinked octahedrally coordinated anionic metal oxyhydroxide surfaquo complexes which form an open network structure. The latter contains considerable quantities of water molecules which facilitate hydroxide ion discharge at the metal site during active oxygen evolution, and also charge compensating cations. The dynamics of redox switching has been quantified via analysis of the cyclic voltammetry response as a function of potential sweep rate using the Laviron-Aoki electron hopping diffusion model by analogy with redox polymer modified electrodes. Steady state Tafel plot analysis has been used to elucidate the kinetics and mechanism of oxygen evolution. Tafel slope values of ca. 60 mVdec-1 and ca. 120 mVdec-1 are found at low and high overpotentials respectively, whereas the reaction order with respect to hydroxide ion activity changes from ca. 3/2 to ca. 1 as the potential is increased. These observations are rationalised in terms of a kinetic scheme involving Temkin adsorption and the rate determining formation of a physisorbed hydrogen peroxide intermediate on the oxide surface. The dual Tafel slope behaviour is ascribed to the potential dependence of the surface coverage of adsorbed intermediates.

1. INTRODUCTION

In recent years there has been a renewal in interest in the oxygen evolution reaction (OER) at transition metal oxide based electrodes in alkaline solution. Alkaline water electrolysis has been

proposed as an environmentally inoffensive route to the production of the large volumes of hydrogen gas required by a possible hydrogen economy [1-5].

In practice, the efficiency of water electrolysis is limited by the large anodic overpotential of the oxygen evolution reaction (OER) [5]. Currently, the optimal OER anode materials are RuO_2 and IrO_2, since these oxides exhibit the lowest overpotentials for the OER at practical current densities [6]. However, the high cost of these materials and their poor long term stability in alkaline solution renders their widespread commercial utilisation both uneconomical and impractical [7].

In light of these limitations, the oxides of the first row transition metals offer a compromise solution. Although they possess inferior electrocatalytic activity for the OER, their relatively low cost and long term corrosion resistance in alkaline solution makes them attractive OER anode materials [7-10].

Despite this revival of interest the mechanism of the OER at first row transition metal oxide surfaces remains controversial and the question of a possible common mechanism, which would facilitate a theory of electrocatalysis for oxygen evolution, is therefore unresolved. It is our opinion that a systematic and consistent study of the OER at the oxidised surfaces of electrodes of adjacent first row transition metals should prove useful in elucidating whether a common reaction mechanism prevails.

At present there exists a significant body of work on the oxygen evolution electrocatalytic properties of oxidised Ni electrodes [8, 11-19], while several independent workers have investigated the details of the reaction at oxidised Co anodes [9, 20-23]. In contrast, to the best of our knowledge, the work of Lyons *et al.* [10, 24, 25] and an early comparative study by Scarr [26] are the only meaningful studies on the kinetics of the OER at oxidized Fe substrates.

In the present paper we examine the mechanism of anodic oxygen evolution at oxidized iron electrodes in alkaline solution using a combination of steady state polarization techniques and reaction order studies. We propose a mechanism for the latter which specifically takes the nature of the electrochemically generated hydrous iron oxide film that is present on the surface of the Fe electrode during active oxygen evolution into account.

In this work, we focus on the oxygen evolution electrocatalytic behaviour of polymeric iron oxyhydroxide electrodes.

A duplex layer model in which the oxide/solution interface consists of a compact anhydrous inner layer and a micro-dispersed hydrous outer layer has been proposed by Burke and coworkers [28, 29].

This model envisages that the ions of the inner region are held in place by a rigid network of polar covalent bonds through which ionic transport is difficult whereas charge percolation proceeds comparatively easily and quickly through the outer, hydrous, polymeric oxide region.

Indeed, Lyons and Brandon [25] have recently calculated that the average rate of charge diffusion for a hydrous oxide covered Fe electrode in base is comparable to that of poly(pyrrole). In the present paper the effect of hydrous oxide layer thickness on the kinetics of the oxygen evolution reaction (OER) will be examined with a particular emphasis placed on hydrous iron oxide in aqueous alkaline solution.

2. EXPERIMENTAL

2.1 Electrochemical cell

All experiments were conducted in a conventional three electrode cell. The working electrode was constructed from 1mm thick polycrystalline iron foil (as supplied by Alfa Aesar-Johnson Matthey, purity 99.9945% (metals basis)) with a geometric surface area of 0.16 cm^2. Prior to each experiment the surface of the working electrode was polished successively with 1200 grit carbimet paper and a slurry of 0.3 micron alumina powder until a "mirror bright" finish was achieved. A platinum wire electrode (CH Instruments, cat no. CHI 115) was employed as the counter electrode and a mercury-mercuric oxide (Hg/HgO) reference electrode (CH Instruments, cat no. CHI 152) was utilised as the reference standard, therefore all voltages are quoted against this reference electrode. A 0.5 M NaOH solution served as both the electro-polymerization medium and the supporting electrolyte for the redox switching and electro-catalytic studies. This solution was prepared from sodium hydroxide pellets (Sigma-Aldrich, minimum 99% purity) using Millipore water (resistivity > 18 MΩ cm). Before commencing each experiment, nitrogen gas was bubbled through the electrolyte solution for 20 min.

2.2 Electrochemical measurements

All electrochemical data was recorded digitally using either a BAS 100B Electrochemical Analyser or a CHI 760D bipotentiostat, both of which were interfaced to a personal computer. The uncompensated solution resistance was determined using chronoamperometry. The current response to a small potential step (50 mV) was recorded in a potential region where no faradaic processes were occurring. The solution resistance was then calculated using the relationship $i = (\Delta E/R)\exp\left[-\dfrac{t}{R_u C_{DL}}\right]$ where ΔE is the magnitude of the potential step (V), R_u is the uncompensated solution resistance (ca. 0.60 Ω for [OH⁻] = 0.5 M), t is time (s) and C_{DL} is the double layer capacitance (F). Accordingly, the steady state polarization plots were corrected for the *iR* drop. Unless otherwise specified, all values of current density are normalized with respect to the geometric surface area.

The polymeric Fe oxyhydroxide films were prepared *via* multicycling the Fe electrode between the switching potentials of -1.30 V and 0.75 V at a scan rate of 0.40 V s^{-1}. Films of different thicknesses were prepared by varying the number of growth cycles. The charge storage capacity or redox capacity (Q) was determined, following the growth of each film, by integration of the peaks in a voltammetric profile recorded at a slow sweep rate (40 mV s^{-1}). The redox capacity is directly proportional to the layer thickness. Tafel plots were recorded for each film using linear sweep voltammetry performed at a sweep rate of 1 mV s^{-1}.

3. RESULTS AND DISCUSSION

3.1 Hydrous Oxide growth via repetitive potential sweep multicycling (RPSM)

One of the most versatile and convenient techniques used to generate hydrous oxides in a

form suitable for the real time determination of their redox switching and electrocatalytic behavior is that of potential cycling . In this method the potential of an electrode of the parent metal (which may be noble or non-noble) is cycled repetitively between suitable lower and upper limits in an aqueous solution of appropriate pH. The type of potential perturbation used for oxide growth – sinusoidal, square or triangular wave- apparently makes little difference . Indeed the triangular wave is most convenient as changes in the current vs potential response (the voltammogram) can be employed during the oxide growth reaction to monitor changes in redox behavior associated with the latter as illustrated in fig.1(a) for the growth of hydrous oxide thin films on Fe electrodes in aqueous alkaline solution (0.5 M NaOH). The experimental conditions used during the multicycling procedure have been optimised previously [30] and the peak designations utilised here were defined in the latter work. It is clear that peaks A_3 and C_2 are the only peaks that display a significant enhancement on repetitive cycling. In simple terms peaks A_3/C_2 can be attributed to the following Fe(II)/Fe(III) redox transformation:

$$Fe(OH)_2 + OH^- \rightarrow FeOOH + H_2O + e^-$$
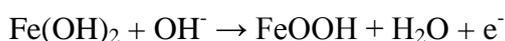
However, it was previously shown that the A_3/C_2 peaks exhibit the usual characteristic of a hydrous or hyper-extended oxide [30], i.e. *a super-nernstian potential-pH shift*, which has the value of $dE/dpH = -2.303(3RT/2F) = -0.088V/pH$ unit at T = 298 K. Accordingly, by analogy with a scheme produced by Burke and Whelan [31] for redox switching of iridium oxide films, it has been proposed that the main redox switching reaction may be written as:

$$[Fe_2(OH)_6(OH_2)_3]_n^{2-} + 3nOH^- \rightarrow [Fe_2O_3(OH)_3(OH_2)_3]_n^{3-} + 3nH_2O + 2ne^-$$

corresponding to an Fe(II)/Fe(III) redox transition in a polymeric microdispersed hydrous oxide layer. This redox switching reaction is illustrated schematically in scheme A below.
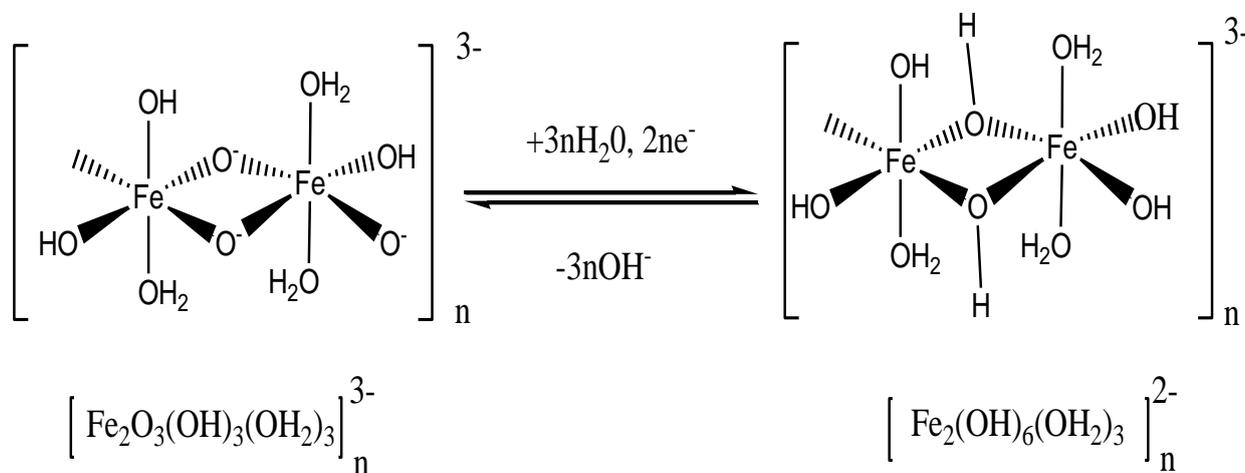
Scheme A

The growth of the hydrous oxide film was monitored by following the development of these redox peaks as a function of the number of cycles N[1]. The variation in the voltammetric charge capacity Q (determined by integration of the voltammetric peak A_2) as a function of N is outlined in Figure 1b. Experimentally, it was found that the charge tends toward a constant limiting value as N is increased. We have been able to fit the latter charge capacity vs number of growth cycles data to a physically meaningful analytical expression which is: $Q = a\{1 - \exp[-bN]\}$. The pertinent NLLS fitting parameters are included as an inset in fig.1 (b) below.
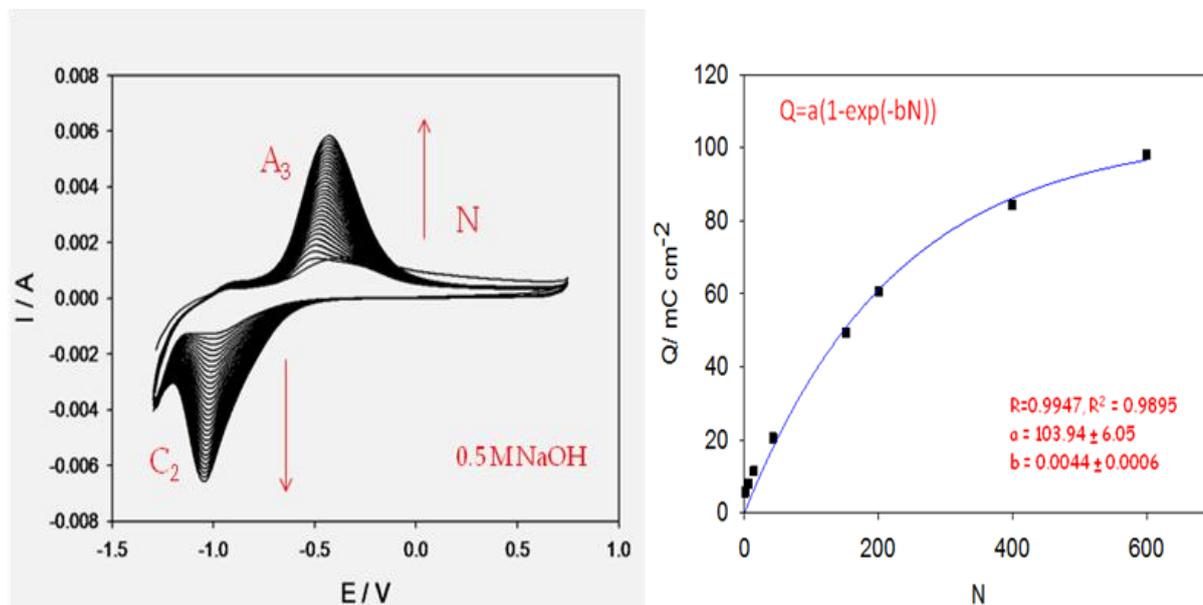
Figure 1. (a) Growth of hydrous iron oxide thin film on Fe support electrode monitored via analysis of the evolution of the real time voltammogram in 0.5 M NaOH. (b) Variation of charge capacity obtained via integration of A_3 peak as function of number of oxide growth cycles N.

The mechanism of hydrous oxide growth on repetitive potential cycling is now reasonably well understood, at least at a qualitative level and has been discussed by Lyons and Burke [30] and by Pickup and Birss [32]. It may be assumed that the initial oxidation process involves the formation of OH and O radicals which adsorb, initially in a reversible manner on the metal surface. With increasing degree of surface coverage adsorption assumes a more irreversible character accompanied by the formation, via a place exchange mechanism, of a thin, largely anhydrous, compact passivating phase oxide layer . Under conventional steady state anodization conditions such layers are usually of limited thickness as the activation energy for atom or ion migration in the compact film is generally quite large. However there are some exceptions, e.g. molybdenum has been shown to oxidize at a steady rate at quite low potentials – evidently in this case the oxide produced rearranges readily to a crystalline form, rather than remaining as a compact amorphous layer.

---

[1] This type of real time monitoring of the chemical modification of an electrode surface during in situ electro-polymerization has also been used extensively in the field of electroactive polymer electrochemistry.

Even though it is directly produced in the initial electrochemical oxidation process, the anhydrous film is probably not the most stable metal oxidation product in the aqueous medium but it may be regarded as an intermediate or metastable product in the formation of a hydrous oxide layer. In the anhydrous film ions are held in a rigid manner in an extended network of polar covalent bonds which drastically reduce ion transport through (and consequently extension of) the surface layer.

The next stage of the film thickening process, the hydration reaction, is generally very slow, because as in phase transformation reactions, it involves rupture of primary coordination metal-oxygen bonds. It has been shown that the extent of hydrous oxide growth depends strongly on the value chosen for the upper and lower limit of the potential sweep as well as on the cycling frequency adopted, the solution temperature and the solution pH.

The marked dependence of oxide growth rate on the lower limit of the potential sweep is indicative of the essential role that partial reduction of the anhydrous oxide plays in the production of a thick deposit.

Partial reduction of the compact oxide layer apparently facilitates rearrangement of oxycation species at the metal surface, leaving it in a somewhat disrupted state. It is established that in the case of both platinum [33] and gold [34, 35] the anhydrous film is reduced much more readily than the hydrated film. The greater stability of the latter is possibly due to a variety of reasons such as lower repulsion between cations owing to greater separation and decreased charge (the latter effect being due to hydroxyl ion coordination by cations present) and polymer formation. Indeed it has been established that in the case of metal-gas interactions [36] the adsorption-desorption process effects displacement of atoms in the outer layer of the metallic phase, and that potential cycling causes roughening of the surface of noble metals such as platinum under certain conditions [37].

On subsequent re-oxidation of the partially reduced metal surface the compact layer is restored but the outer region of the compact film is present in a more dispersed form. On further reduction the latter material becomes incorporated into the hydrated outer layer. It is not clear whether this rearrangement process involves detachment of oxycations, i.e. a dissolution-reprecipitation mechanism, or a certain weakening, with only a partial detachment of oxycation binding in the compact oxide layer. In the latter case the partially reduced cations are assumed to be displaced from normal lattice sites, and, as such, are more susceptible to oxidation in the subsequent anodic sweep during which they complete their oxygen coordination shell of six oxygen atoms to form a rather open polymeric inorganic bronze or zeolite type structure. Hence under conditions of thick film growth the interfacial region may be represented by : $M/MO_x/MO_a(OH)_b(OH_2)_c$/aqueous phase as is outlined in figure 2. This is the duplex layer model of the oxide/solution interphase region. Here MO_x represents the inner compact layer and $MO_a(OH)_b(OH_2)_c$ denotes the outer hydrous layer. This model was first suggested by Burke and O'Sullivan [38].
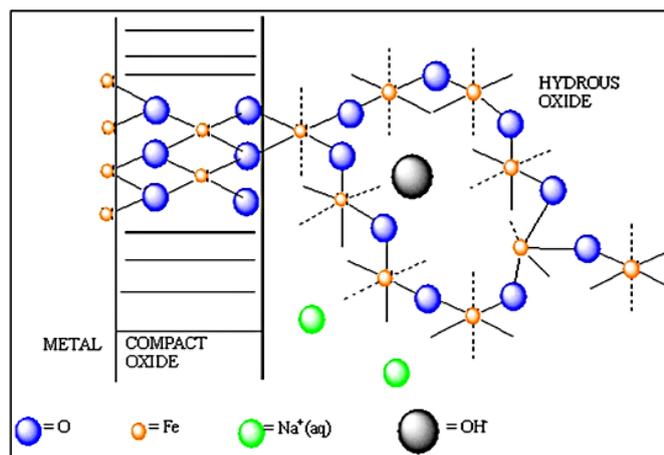
Figure 2. Schematic representation of the Burke-O'Sullivan Duplex Layer Model of the oxide-solution interface.

The upper limit of the potential sweep has also an important effect on the rate of oxide growth. The importance of this parameter probably lies in the fact that it extends oxygen penetration into the outer regions of the metal lattice. It may also help to generate a slight expansion and stress associated disruption at the metal-oxide interface. The upper limit may also facilitate uptake of a slight excess of oxyhen by the oxide phase. It has often been observed that there is an optimal value of upper limit : hydrous oxide growth (as manifested by oxide charge capacity Q) is less at values more cathodic and indeed more anodic than this optimal value. The fall off in oxide growth efficiency at more anodic values of upper potential limit may be possibly associated with the increasing difficulty of reduction of the surface – which is likely to be considerably passivated at more extreme anodic potentials -- at lower potentials. Indeed it has been established that the oxide reduction reaction involves a nucleation process which occurs less rapidly as the film formation potential is raised [39]. Hence the optimum upper limit probably corresponds to a potential which represents the best compromise between two opposing effects, e.g. the compact layer must attain a reasonable thickness (hence the need for a relatively high anodic potential), but too high an upper limit results in a very unreactive layer which does not reduce readily at the lower potential limit.

In summary, for most metals, but especially gold, platinum, iridium and rhodium, extension of oxide growth beyond the monolayer level under conventional galvanostatic or potentiostatic conditions is usually quite slow. This is obviously due to the presence of the initial compact oxide product layer which acts as a diffusive barrier to further growth (such compact oxides often exhibit parabolic growth kinetics). Under potential cycling conditions the upper limit plays a significant role. There is probably a combination of thermodynamic and kinetic factors involved, but evidently the upper limit must be sufficiently anodic that compact oxide formation exceeds significantly the single monolayer level so that on subsequent reduction, a disturbed, highly disordered layer of metal atoms is prepared on the electrode surface (fig.2). Thus with platinum [40] and gold [41], two metals where oxide monolayer behaviour is well defined, the optimum

lower limit lies at a potential value at, or below, the value of the monolayer oxide reduction peak.. On subsequent reoxidation the disturbed layer of metal atoms is evidently converted to hydrated, or partially hydrated oxide – complete hydration under these circumstances may involve several redox cycles – with a fresh inner compact layer being regenerated at the metal surface on each anodic sweep. On repetitive cycling the porous outer layer increases in thickness at the expense of the underlying metal. Lack of stirring dependence in such oxide growth reactions suggests that solution species, i.e. a dissolution/hydrolysis mechanism, are not involved.

3.2 Oxygen evolution reaction steady state polarisation measurements

Our investigations of the electrocatalytic properties of hydrated iron oxyhydroxide layers have focussed on the technologically important oxygen evolution reaction (OER). The relatively large magnitude of the anodic oxygen evolution overpotential at a given operational current density, is the principal factor limiting the efficiency of industrially important cathodic processes such as metal electrowinning and hydrogen production via alkaline water electrolysis. There has, consequently, been considerable research effort devoted to decreasing oxygen evolution overpotentials, through the development of novel anode materials. Some of the more recent reviews of the OER, include those due to Kinoshita [7] and Gattrell and MacDougall [42]. It is worth noting that in alkaline solution, oxygen evolution may be described via the following stoichiometric equation:

$$4\,OH^- \rightarrow O_2 + 2H_2O + 4e^- \tag{1}$$
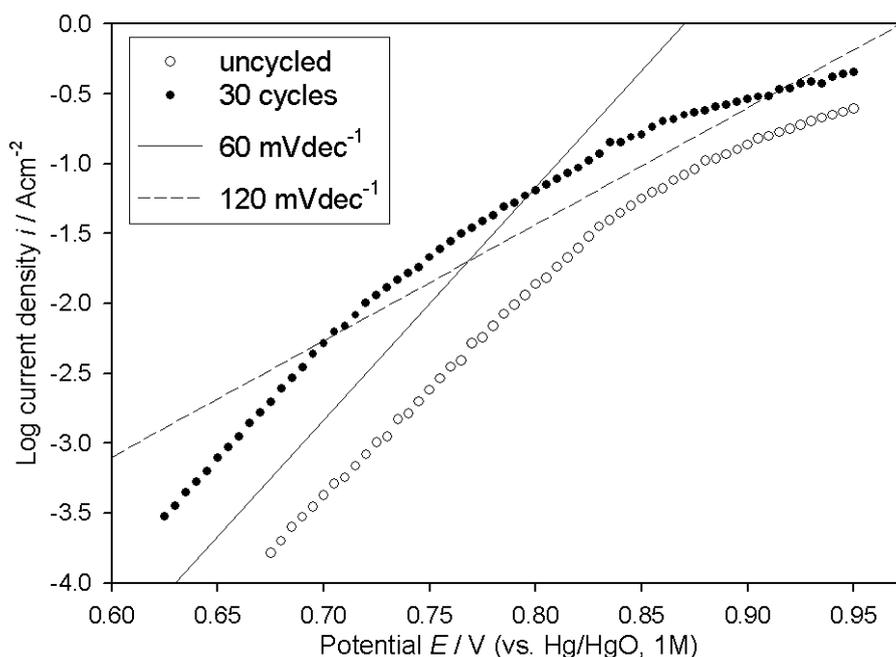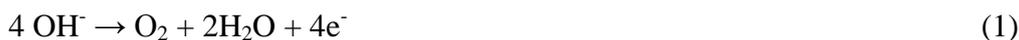
Figure 3. Comparison of *iR* corrected, oxygen evolution steady state polarisation curves for a multi-cycled (30 cycles, − 1.425 to 0.325 V (vs Hg/HgO), 0.35 Vs^{-1}) and an uncycled iron electrode in 1.0 M NaOH at 25ºC.

A comparison is presented in Fig. 3, of *iR* corrected, OER steady state polarisation curves recorded in 1.0 M NaOH solution, for an uncycled and a multi-cycled polycrystalline iron electrode. The multi-cycled electrode was prepared by cycling the electrode potential between limits of −1.425 and 0.325 V (30 cycles) in 1.0 M NaOH at a sweep rate of 0.35 Vs^{-1}. The Tafel plots of Fig. 20 reproduce and therefore confirm a result that was first published by us some time ago [24] and again more recently [10,43], namely that the oxygen evolution performance of a multi-cycled Fe electrode is significantly enhanced relative to an uncycled electrode. In that preliminary communication, the rate of the OER in 1M NaOH was observed to increase by a factor of ten for a multi-cycled Fe electrode (as in the present work, $Q \approx 30$ mC cm^{-2}) by comparison with an uncycled anode, for potentials associated with the lower straight line Tafel region. A similar conclusion can be drawn from the data of Fig. 20, with an OER current density of $i = 5.6$ mAcm^{-2} recorded for the multi-cycled electrode at $E = 0.7$ V, while at the same potential for the uncycled electrode, $i = 0.42$ mAcm^{-2}. Subsequent to our publication on oxygen evolution at multi-cycled Fe electrodes, it was shown by Gennero De Chialvo and Chialvo [18,23] that the rate of the OER in aqueous alkaline solution is also enhanced for multi-cycled Ni and Co anodes relative to uncycled electrodes of the same metal, although these workers did not offer any mechanistic rationalisation of their kinetic data.
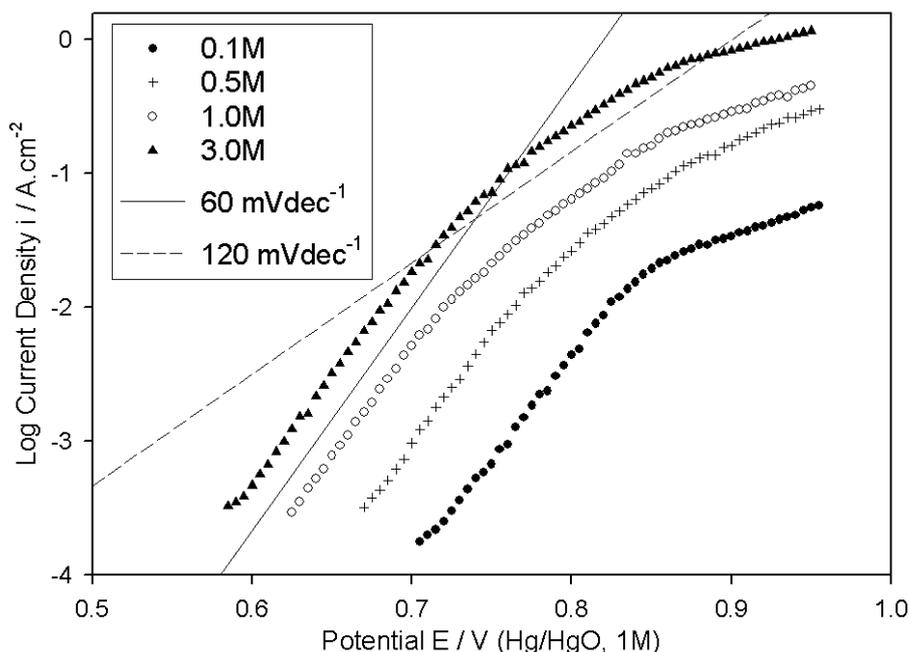

Figure 4. *iR* corrected steady state polarisation curves recorded in the direction of increasing potential for a for a multi-cycled (30 cycles, − 1.425 to 0.325 V, 0.35 Vs^{-1}) iron electrode in NaOH solutions of various concentration.

It should also be pointed out at this stage that the OER does not occur on a metallic surface in the case of the uncycled Fe electrode − upon introduction to alkaline solution and application of

an anodic polarisation regime, a passive oxide will form on the metal surface, and it is at the surface of this oxide that electrocatalysis of the OER occurs. As we discussed previously [10,43], it is likely that the principal reason behind the increase in OER electrocatalytic activity, on going from an uncycled to a multi-cycled Fe anode, is related to the significant increase in oxyiron – solution contact, which will accompany the thickening (with potential cycling) of the porous, dispersed, outer hydrous oxide.

The effect of solution OH⁻ ion concentration (at a constant hydrous oxide layer thickness) on the rate and kinetics of the OER is detailed in Fig. 4. For each experiment, the oxide layer was grown for 30 cycles in 1.0M NaOH as described above, and the electrode was then transferred to the test solution. The interesting features of the data of Figs. 3 and fig. 4 are as follows. Firstly, a Tafel slope, b, of ca. 60 mVdec^{-1} ($\approx$ 2.303 $\times$ RT/F at 25ºC) is observed at lower potentials, regardless of base concentration and for both the multi-cycled and uncycled electrodes. This indicates that in this region of potential, the nature of the rate determining step (RDS) remains invariant with respect to oxide thickness and nature (i.e. thick hydrous oxide vs. thinner passive oxide) or OH⁻ ion concentration. WE will comment further on this subsequently. There is also evidence for a second Tafel region (slope ca. 120 mVdec^{-1} $\approx$ 2.303 $\times$ 2RT/F at 25ºC) at higher overpotentials. This observation must arise naturally from the quantitative analysis of any proposed mechanistic scheme. Deviations from ideal Tafel behaviour are observed at still higher potentials. This presumably arises due to the onset of mass transport limitations.
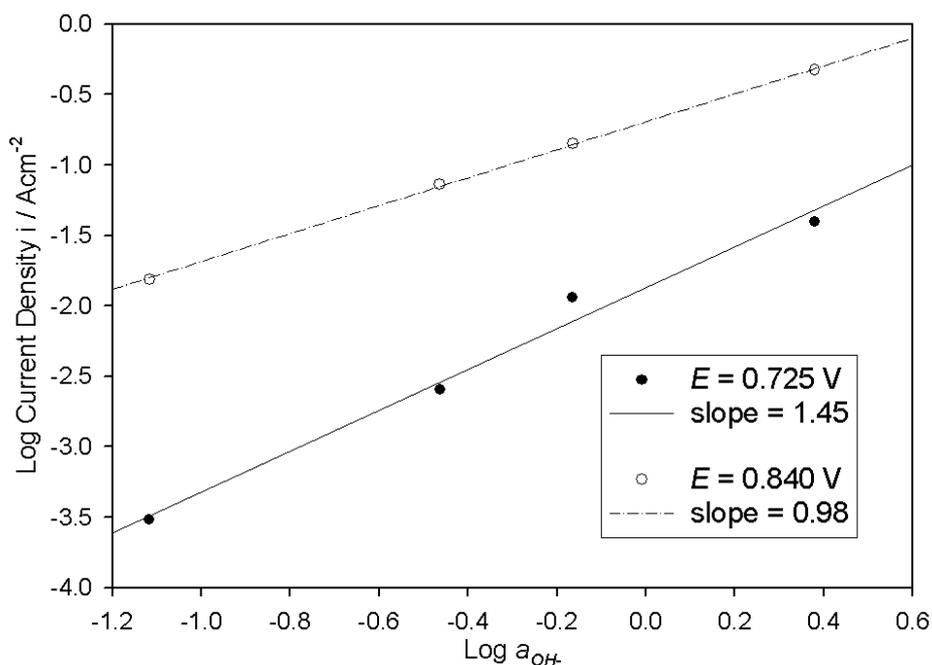

Figure 5. Reaction order plots based upon the polarisation curves of Fig. 21, at the indicated potentials.

A reaction order plot with respect to OH⁻ ion activity (calculated from literature values [44]

for the mean ionic activity coefficients, $\gamma_\pm$) is constructed in Fig. 5 for a potential (0.725 V) located in the lower Tafel slope region. The significant feature here is that a non-integral reaction order, m_{OH^-}, of ca. 3/2 is obtained. Similar numerical values for the reaction order are obtained for plots derived from current density data recorded at other potentials in the low Tafel slope region. In contrast, we also note from Fig. 5 that a reaction order of approximately unity is obtained for data extracted from the higher Tafel slope region (0.850 V).

Typical Tafel plots for the OER recorded in 0.5 M NaOH solution as a function of oxide charge capacity (as determined by varying the number of oxide growth cycles) are illustrated in figure 6. It is clear that the current density, especially in the high Tafel slope region measured at a fixed potential increases with increasing oxide layer thickness. Also the region of Tafel linearity in the low potential region becomes more narrow as the thickness of the hydrous oxide is increased. Furthermore, as outlined in figure 7, the Tafel slope recorded at low potentials varies in a regular manner with oxide charge capacity.
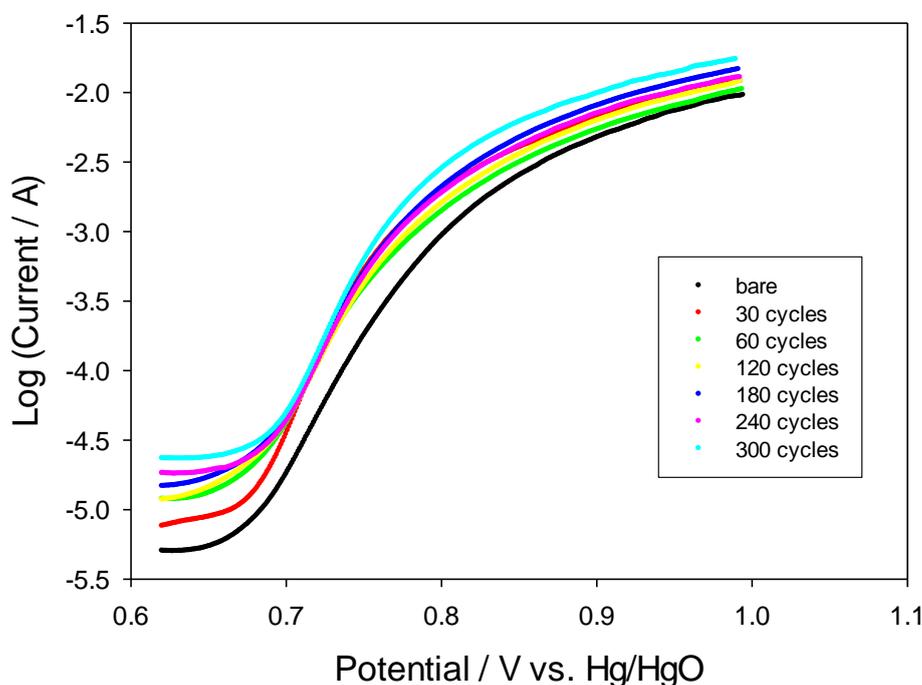

Figure 6. iR corrected Tafel plots for the OER recorded in 0.5 M NaOH for multicycled iron electrodes at various oxide layer thicknesses.

A clear variation from ca. 60 mV/dec for an uncylcled electrode, to ca. 40 mV/dec for an electrode coated with a thick oxide layer may be discerned. It is also interesting to note that the threshold potential between the low Tafel slope region and the high Tafel slope region decreases smoothly with increasing hydrous oxide charge capacity. This type of behaviour has been previously noted by Burke and O'Sullivan [45,46] for rhodium in base where it was noted that the Tafel slope recorded at low potentials (ca. 1.40 – 1.57 V (vs RHE)) for the OER decreased gradually from a value of ca. 75 mV/dec for an electrode free of any thick film, to a limiting value

in the region of ca. 47 mV/dec for a surface coated initially with a thick hydrous oxide layer. At higher potentials (ca. 1.57 – 1.76 V (vs RHE)) a Tafel slope of ca. 120 mV/dec was observed for all oxide layer thicknesses. It was further noted that the potential defining the transition between the low and high Tafel slope region decreased smoothly with increasing oxide charge capacity.

We agree with the analysis proposed by Burk and O'Sullivan [45,46] that the gradual lowering of the low potential Tafel slope value with increase in oxide charge capacity could well suggest that hydrated oxide formation occurs initially by an 'island' mechanism – the lower slope being reached when the metal surface is completely covered with hydrous oxide. Alternatively, and this is more probable, the change could well be due to a gradual increase in the extent of hydration of a film of uniform thickness, at low values of the latter, with increasing charge storage capacity. The higher slope in the case of the uncycled electrode surface suggests the operation of weaker hydroxyl coordination of the intermediate at the largely anhydrous compact oxide on this surface, so that the rate of oxygen evolution is not determined exclusively by interaction between the intermediates, as seems to be the case on the hydrated film. Hence the initial fast OH^- ion discharge may have a greater influence on the kinetics of the overall OER process in the case of thinner, less hydrated films. Furthermore the fact that the change in Tafel slope between the first and second regions occurs at lower potentials in the case of thicker films, suggests that limiting coverage of intermediates is observed at lower potentials in the case of the more hydrated films. This is readily understandable on the basis that increased intermediate stability (as reflected in the decrease of Tafel slope) leads to saturation coverage at progressively lower potentials as oxide charge capacity develops until a constant 40 mV/dec slope is observed.
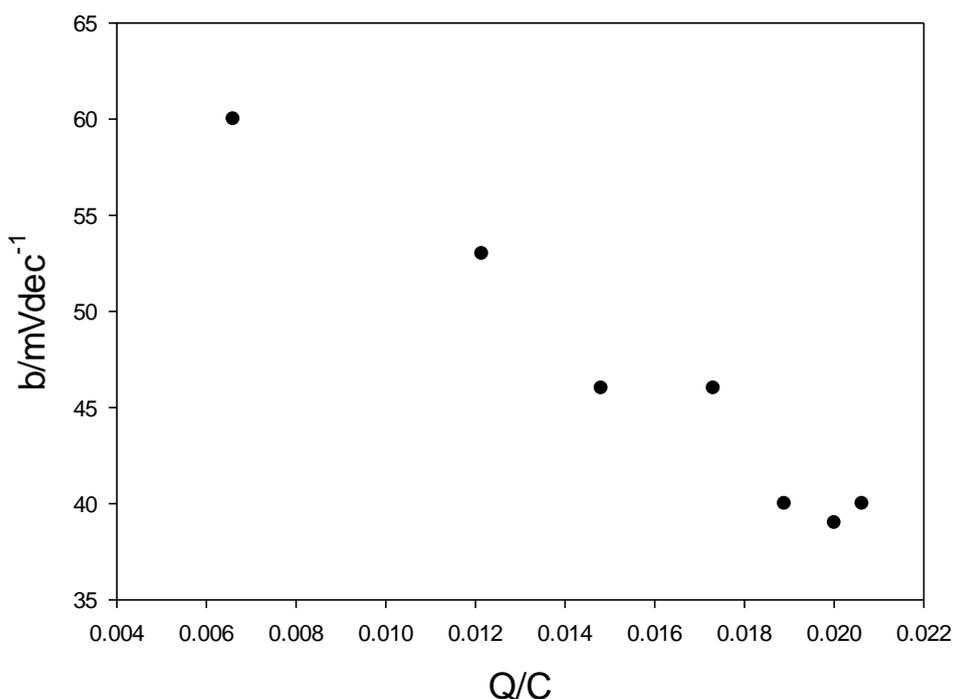

Figure 7. Variation of steady state Tafel slope values recorded at low potentials in OER region as a function of oxide redox charge capacity. Polarization data presented in fig.6.

Furthermore the increase in oxygen evolution rate (manifested as current density recorded at fixed potential E = 0.72 V (vs Hg/HgO)) with increasing oxide charge capacity, in the low Tafel slope region, in the case of the multi- cycled iron electrodes is quite interesting (figure 8) in that it suggests that this is due to increasing electrode real area, i.e. the charge is proportional to the mass of the film, which is, for a microporous layer, linearly related to surface area. Furthermore as noted in fig.9 the oxygen evolution potential recorded at a fixed OER rate of 1.0 mA/cm^2 is seen to decrease significantly as the hydrous oxide redox charge capacity increases. Hence the OER requires less driving force to occur at the same rate as the thickness of the hydrated layer increases. The system becomes more electrocatalytically efficient with increasing oxide redox charge capacity.
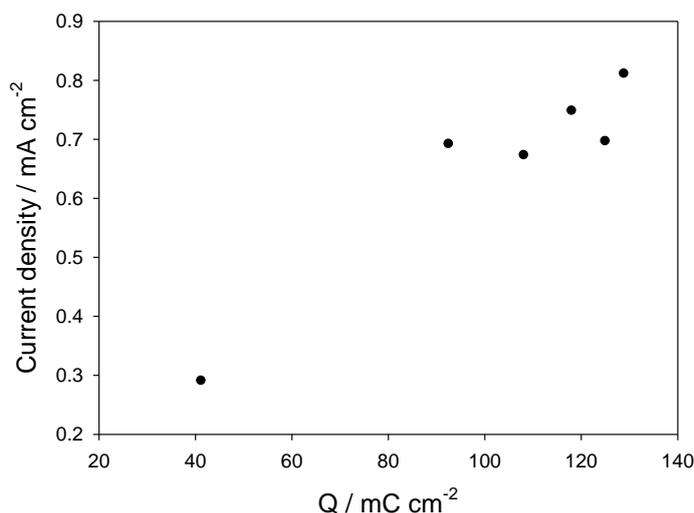
Figure 8. Variation of OER rate expressed as a current density measured at E = 0.72 V which is in the low Tafel slope region as a function of oxide redox charge capacity Q. Polarization data presented in fig.6.
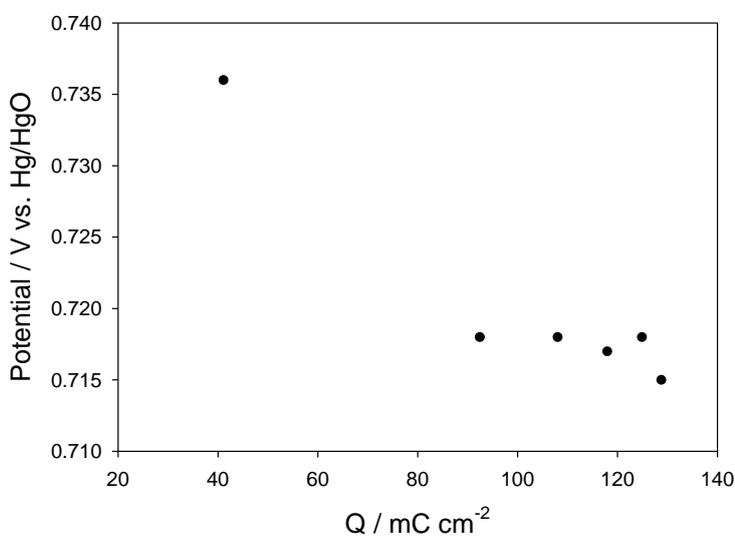
Figure 9. Variation in the potential recorded in the low Tafel slope region corresponding to a fixed OER rate of 1.0 mA/cm^2 as a function of oxide redox charge capacity Q. Polarization data as presented in fig.6.

The variation in threshold potential between the low and high Tafel slope region as a function of hydrous oxide redox charge capacity is presented in fig.10.
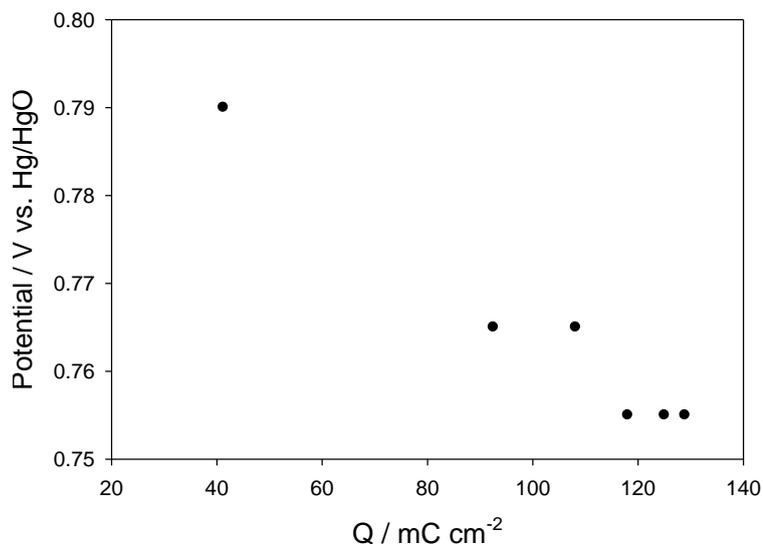
Figure 10. Variation in the low/high Tafel slope switch-over potential as a function of oxide redox charge capacity Q. Polarization data as presented in fig.6.

Finally, we note from fig.11 that the Faradaic current at a potential of ca. 0.65 V increases regularly with increasing oxide charge capacity.
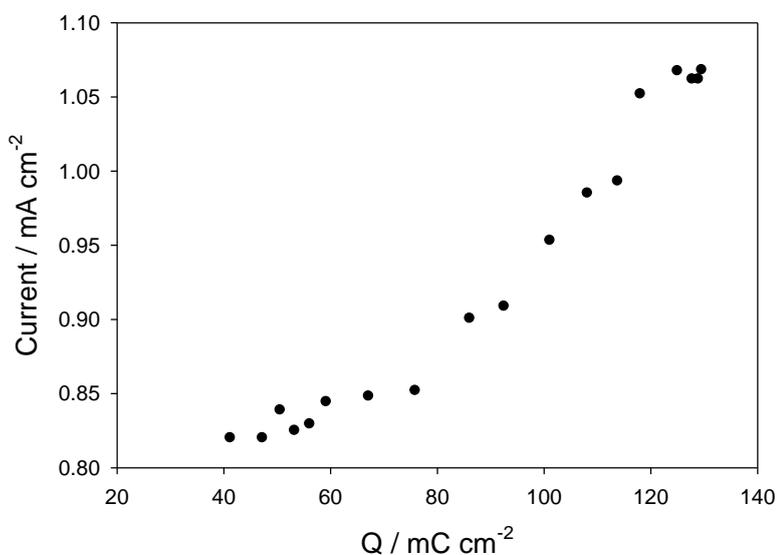
Figure 11. Variation in the current density recorded at a fixed potential of E = 0.65 V just prior to the onset of active oxygen evolution as a function of oxide redox charge capacity Q. Polarization data as presented in fig.6.

A Tafel slope of ca. 120 mV/dec is observed at more elevated anodic potentials for all values of charge capacity, whereas the slope measured at less anodic potentials varies from ca. 60 mV/dec to ca. 40 mV/dec as the redox charge capacity increases. The switchover potential decreases smoothly with increasing redox capacity value.

In summary, a kinetic analysis and associated reaction mechanism for the OER at both the uncycled and multicycled Fe electrodes considered in this article, must predict that $b = 2.303 \times RT/F$ and the reaction order $m_{OH^-} = 3/2$ at low potentials, changing to $b = 2.303 \times 2RT/F$ and $m_{OH^-} = 1$ at higher potentials.

A plausible mechanism recently proposed by Lyons and Brandon [10,43] is outlined as follows. The first two steps in the process are given by,

$$S + OH^- \rightarrow S\text{-}OH + e^- \tag{2}$$

$$S\text{-}OH + OH^- \rightarrow S\text{-}\text{-}H_2O_2 + e^- \tag{3}$$

where $S\text{ -}H_2O_2$ represents *physisorbed* hydrogen peroxide. The physisorbed intermediate is then catalytically decomposed according to the following sequence of reactions:

$$S\text{ -}H_2O_2 + OH^- \rightarrow S\text{- -}HO_2^- + H_2O \tag{4}$$

$$S\text{-}\text{-}H_2O_2 + S\text{- -}HO_2^- \rightarrow O_2 + H_2O + OH^- \tag{5}$$

This type of pathway was first devised by Bockris and Otagawa [47] for perovskite anodes in alkaline solution. We have however, more recently proposed a more general mechanism which specifically utilizes the concept of interlinked octahedral surfaquo groups in an extended polymeric framework [10,43]. We shall see that this mechanism is consistent with the available kinetic data and also with recent spectroscopic [48] experiments. The scheme involves an Fe(VI) hydroperoxy intermediate, and is outlined below. In the scheme potlined below the catalytically active and intermediate species are represented as complex anionic entities, where, in the present case p=2m+n-6. We believe that this approach is more realistic than thinking in terms of discrete simple stoichiometric oxy-hydroxide species.

$$[Fe(VI)O_m(OH)_n]^{p-} + OH^- \rightarrow [Fe(VI)O_{m+1}(OH)_{n-1}]^{p-} + H_2O + e^- \tag{6}$$

$$[Fe(VI)O_{m+1}(OH)_{n-1}]^{p-} + OH^- \rightarrow [Fe(VI)O_m\underline{OOH}(OH)_{n-1}]^{p-} + e^- \ldots RDS \tag{7}$$

$$[Fe(VI)O_m\underline{OOH}(OH)_{n-1}]^{p-} + OH^- \rightarrow [Fe(VI)O_m\underline{OO}(OH)_{n-1}]^{p-} + H_2O + e^- \tag{8}$$

$$[Fe(VI)O_m\underline{OO}(OH)_{n-1}]^{p-} + OH^- \rightarrow [Fe(VI)O_m(OH)_n]^{p-} + O_2 + e^- \tag{9}$$

We have previously noted that the oxide film produced by the potential multi-cycling of an Fe electrode will be significantly more hydrated than that obtained by the passivation of relatively un-aged Fe surfaces. The amount of amphoteric character displayed by an anodic oxide is expected to be proportional to its degree of hydration. It is therefore expected that "aged" and multi-cycled Fe electrodes would contain a larger surface density of the catalytically active, complex anionic $[Fe(VI)O_m(OH)_n]^{p-}$ species at lower overpotentials, relative to fresher Fe electrodes. Note that the concept of the catalytically active site existing in the form of an hydroxylated anionic surface complex is maintained – for Fe(VI), $p = 2m+n-6$. Indeed, since Fe(VI) species (probably in the form of FeO_4^{2+}) are soluble in aqueous alkaline solution , their stabilization on the oxide surface by the coordination of excess OH^- ions provides a tentative explanation as to how they can act as OER active centres. Lyons and Brandon [10,43] noted that the OER pathway defined in eqn. 6 – eqn. 9 above is also suitable for Co anodes, except in this case the active site is represented as $[Co(IV)O_m(OH)_n]^{p-}$ ($p = 2m+n-4$), in agreement with the proposal of Gennero De Chialvo et al. [18,23] that the catalytic species is likely to exist as discrete CoO_2 entities.

3.3 Steady state kinetic analysis of multi-cycled Fe electrodes in aqueous base

We now proceed with a kinetic analysis of the mechanism presented generally in eqn.6 to eqn.9, and assume that at lower overpotentials there prevails an *intermediate coverage* of S-OH species. Therefore a *Temkin adsorption isotherm* is applicable [49-52]. This approach differs from our previous analysis [10] where a Langmuir adsorption isotherm was assumed. We adopt a similar approach to the application of the Temkin isotherm, as that taken by Damjanovic et al. [53] in an important early work on OER kinetics. These workers based their analysis of coverage effects due to adsorbed intermediates, on the principle that a decrease in the free energy of adsorption of an intermediate species (with increasing total coverage) that is a product of a given step, results in an increase in the free energy of activation for that step. In contrast, a decrease in the free energy of adsorption of an intermediate species (again with increasing overall coverage), which is a reactant in a particular step, will cause a decrease in the free energy of activation for the step. In terms of this model the free energy of adsorption of a given species *i*, depends to the total fractional coverage θ_Σ [49,53] of all adsorbed reaction intermediate species on the electrode surface according to,

$$\Delta G_\theta'^0 = \Delta G_0'^0 - g_i \theta_\Sigma \tag{10}$$

since it is the sites remaining beyond the overall fractional coverage that determine, through the respective *g* values, the energy of adsorption that species *i* will experience when adsorbed under such conditions. The term g_i in eqn. 10 is clearly the rate of change of the free energy of adsorption of species *i* with the total coverage. The approach outlined above is useful in the analysis of the situation where there may be two or more adsorbed intermediate species present simultaneously on an electrode surface.

Let us now consider the first electron transfer step in the Lyons Brandon reaction sequence. The forward reaction flux f_1 (units: mol cm^{-2}s^{-1}) is given by:

$$f_1 = k_1'^0 a_{OH} (1 - \theta_{SOH}) \exp\left[\frac{\beta F}{RT}\eta\right] \exp\left[\frac{-\gamma g_{SOH}\theta_\Sigma}{RT}\right] \tag{11}$$

In this expression θ_{SOH} denotes the fractional of the electrosorbed S-OH species formed in step (3) or (7), while γ is a symmetry factor, with $0 < \gamma < 1$ and $\gamma = 1 - \beta$. The reverse desorption step is described by the following expression:

$$f_{-1} = k_{-1}'^0 \theta_{SOH} \exp\left[\frac{-(1-\beta)F}{RT}\eta\right] \exp\left[\frac{(1-\gamma)g_{SOH}\theta_\Sigma}{RT}\right] \tag{12}$$

We assume that at low overpotentials, step (3) or step (7) is rate determining and that the first step is at pseudo-equilibrium. Since an intermediate total fractional coverage is assumed ($0.2 \le \theta_\Sigma \le 0.8$), it is possible, under these conditions, that a significant fractional coverage, $\theta_{SH_2O_2}$, of the intermediate formed in the RDS (S--H$_2$O$_2$) may be achieved. Consequently the net reaction flux must be written as:

$$f_\Sigma = f_2 = k_2'^0 a_{OH} \theta_{SOH} \exp\left[\frac{\beta F}{RT}\eta\right] \exp\left[\frac{(1-\gamma)g_{SOH}\theta_\Sigma - \gamma g_{SH_2O_2}\theta_\Sigma}{RT}\right] \tag{13}$$

The free energy of adsorption for the physisorbed hydrogen peroxide entity formed in the second step is likely to be much less sensitive to the value of the total fractional coverage θ_Σ than is the case for the chemisorbed S-OH species formed in the initial step, and so it is appropriate to assume that $g_{SOH} \gg g_{SH_2O_2}$. In this case eqn. 13 reduces to:

$$f_\Sigma = k_2'^0 a_{OH} \theta_{SOH} \exp\left[\frac{\beta F}{RT}\eta\right] \exp\left[\frac{(1-\gamma)g_{SOH}\theta_\Sigma}{RT}\right] \tag{14}$$

In order to proceed further we invoke the quasi-equilibrium hypothesis to obtain an expression for θ. When quasi-equilibrium prevails we have flux equality $f_1 = f_{-1}$, and so from eqns. 11 and eqn.12 we obtain:

$$\left\{\frac{\theta_{SOH}}{1 - \theta_{SOH}}\right\} \exp\left[\frac{g_{SOH}\theta_\Sigma}{RT}\right] = \frac{k_I'^0}{k_{-I}'^0} a_{OH} \exp\left[\frac{F\eta}{RT}\right] \tag{15}$$

$$= K a_{OH} \exp\left[\frac{F\eta}{RT}\right]$$

For intermediate values of θ_{SOH} the linear pre-exponential term in θ_{SOH} can be assumed to approach unity [50-52], thus yielding the following simplification of eqn. 15:

$$\exp\left[\frac{g_{SOH}\theta_{\Sigma}}{RT}\right] = Ka_{OH}\exp\left[\frac{F\eta}{RT}\right] \tag{16}$$
$$g_{SOH}\theta_{\Sigma} = RT\ln(Ka_{OH}) + F\eta$$

We now substitute this expression for $g_{SOH}\theta_{\Sigma}$ into eqn. 14 to obtain:

$$f_{\Sigma} = k_2'^0 a_{OH}\theta_{SOH}\exp\left[(1-\gamma)\ln(Ka_{OH}) + \frac{(1-\gamma)F}{RT}\eta\right]\exp\left[\frac{\beta F}{RT}\eta\right]$$
$$= k_2'^0 a_{OH}{}^{2-\gamma}\theta_{SOH}K^{1-\gamma}\exp\left[\frac{(1-\gamma+\beta)F}{RT}\eta\right] \tag{17}$$

Taking natural logarithms we obtain:

$$\ln f_{\Sigma} = \ln\left(k_2'^0\theta_{SOH}K^{1-\gamma}\right) + \ln\left(a_{OH}{}^{2-\gamma}\right) + \frac{(1-\gamma+\beta)F\eta}{RT} \tag{18}$$

Setting $\beta = \gamma = 0.5$ achieves:

$$b = \left(\frac{\partial\eta}{\partial\log f_{\Sigma}}\right)_{a_{OH}} = 2.303\frac{RT}{(1-\gamma+\beta)F} = 2.303\frac{RT}{F} \tag{19}$$

$$m_{OH^-} = \left(\frac{\partial\ln f_{\Sigma}}{\partial\ln a_{OH}}\right)_{\eta} = 2-\gamma = \frac{3}{2} \tag{20}$$

Hence, the experimental mechanistic parameters observed at low overpotentials are rationalised.

Furthermore, the high potential behaviour may be explained as follows. The experimentally observed $b = 2.303 \times 2RT/F$ Tafel slope may be ascribed to a change in the surface coverage of adsorbed intermediates at higher potentials to a situation where $\theta_{SOH} \cong \theta_{\Sigma} \to 1$ (i.e. Langmuir isotherm as the total fractional coverage tends to unity). Where Langmuir adsorption conditions prevail, the g_i term in eqn. 14 tends to zero and eqn. 14 thus reduces to:

$$f_{\Sigma} = k_2'^0 a_{OH}\exp\left[\frac{\beta F}{RT}\eta\right] \tag{21}$$

Again taking natural logarithms we obtain:

$$\ln f_{\Sigma} = \ln k_2'^0 + \ln a_{OH} + \frac{\beta F\eta}{RT} \tag{22}$$

Hence the Tafel slope and reaction order are given by (again assuming $\beta = 0.5$):

$$b = \left(\frac{\partial \eta}{\partial \log f_\Sigma} \right)_{a_{OH}} = 2.303 \frac{RT}{\beta F} = 2.303 \times \frac{2RT}{F} \tag{23}$$

$$m_{OH^-} = \left(\frac{\partial \ln f_\Sigma}{\partial \ln a_{OH}} \right)_\eta = 1 \tag{24}$$

The important point to note here is that the dual Tafel slope behaviour is not due to a change in rate determining step, but is due solely to the potential dependence of the total fractional coverage θ_Σ of the electrosorbed reaction intermediates.

At this point, we emphasise the central importance and significance of the fact that the hydrogen peroxide entity formed in step (3) or (7) is envisaged to be physisorbed as opposed to chemisorbed. This is not merely a contrivance to accommodate for the adsorption of intact hydrogen peroxide molecules at the oxide surface. What follows was implicit in the analysis of Bockris and Otagawa [47] when they first outlined this type of OER pathway, however we feel that it is worth stating explicitly.

4. CONCLUSIONS

We now summarise the principal conclusions arising from the present paper regarding the formation, redox properties and electrocatalytic activity with respect to the OER of hydrous oxide coated Fe electrodes in aqueous alkaline solution. First, hydrous microdispersed oxides are readily prepared via the repetitive cyclic potential sweep method applied to the parent metal in aqueous alkaline solution. The latter method is very similar to that employed in the electropolymerization of Electronically Conducting Polymer (ECP) films such as poly(pyrrole) or poly(aniline). The oxide/solution interface has a duplex character, consisting of an inner, largely anhydrous compact oxide, and an outer, hydrated microdisperse oxide layer which exhibits significant electrocatalytic activity with respect to anodic oxygen evolution. Second, the charge storage/charge percolation properties of the hydrous oxide depend on electrochemical and environmental variables such as the lower and upper potential sweep limits, the potential sweep rate, the base concentration employed, the solution temperature, and the solution pH. Third, the acid/ base behaviour of anodically formed transition metal oxides is important when considering the mechanism of both redox switching and oxygen evolution. Furthermore, hydrous oxides are more difficult to reduce than less hydrated compact materials, and this may well have a significant implication for the catalysis of the cathodic ORR.

With respect to the catalysis of the anodic OER process, the sole pathway, that can account for the entire set of experimental parameters observed is the *physisorbed hydrogen peroxide mechanism*. The second step of this pathway, which involves the breaking of a S-OH chemical bond, is considered to be rate limiting. The different values of b and m_{OH^-} observed for the same electrode at different overpotentials, arise due to changes in the fractional coverage θ_Σ of the reaction intermediates, and not due to changes in rate determining step. A similar mechanistic

pathway is likely to prevail for oxidised Ni anodes, except that the OH^- ion that reacts in the rate determining second step originates from the surface anionic complex $[Ni(III)O_m(OH)_{n+1}]^{p-}$ (p=2m+n-3) rather than from the bulk solution . In general it is important to understand that , giving consideration to the acidic nature of hydrated oxide surfaces at high pH, is extremely useful in understanding the OER at transition metal surfaces in aqueous alkaline media. Since in general, the catalytic centres for oxygen evolution reside on the surface of an oxide phase in contact with aqueous solution, the surface region of the oxide will inevitably become somewhat hydrated. In view of this, it is our belief that all workers in this area should consider the amphoteric nature of their oxide surfaces, regardless of how the oxide phase was prepared. It is, for example, to take the case of a Ni anode in alkaline solution, more realistic to represent the OER active site as $[Ni(III)O_m(OH)_n]^{p-}$ (where extra hydroxide ions have been coordinated from solution, owing to the acidic nature of the oxide in electrolytes of high pH), rather than the traditional practice of considering it to be a discrete NiOOH entity.

References

1. K. Zeng and D. Zhang, *Prog. Energy Combust. Sci.,* 36 (2010) 307.
2. H. Tributsch, *Int. J. Hydrogen Energy*, 33 (2008) 5911.
3. G. W. Crabtree, M. S. Dresselhaus and M. V. Buchanan, *Phys. Today*, December 2004, 39.
4. J. Ohi, *J. Mater. Res.,* 20 (2005) 3180.
5. D. E. Hall, *J. Electrochem. Soc.,* 130 (1983) 317.
6. A. Michas, F. Andolfatto, M. E. G. Lyons and R. Durand*, Key Eng. Mater.*, 72-74 (1992) 535.
7. K. Kinoshita, *Electrochemical Oxygen Technology*, Wiley-Interscience, New York, 1992.
8. M. E. G. Lyons and M. P. Brandon, *Int. J. Electrochem. Sci.,* 3 (2008) 1386.
9. M. E. G. Lyons and M. P. Brandon, *Int. J. Electrochem. Sci.,* 3 (2008) 1425.
10. M. E. G. Lyons and M. P. Brandon, *Int. J. Electrochem. Sci.,* 3 (2008) 1463.
11. A.I. Krasil'shchikov, *Zh. Fiz. Khim*. 37 (1963) 531.
12. N. Sato, G. Okamoto, *Electrochim. Acta*, 10 (1965) 495.
13. M.H. Miles, G. Kissel, P.W.T. Lu, S. Srinivasan, *J. Electrochem. Soc.,* 123 (1976) 332.
14. P.W.T. Lu, S. Srinivasan, *J. Electrochem. Soc.,* 125 (1978) 1416.
15. G. Bronoel, J. Reby, *Electrochim. Acta*, 25 (1980) 973.
16. L.D. Burke, T.A.M. Twomey, *J. Electroanal. Chem.,* 167 (1984) 285.
17. B.E. Conway, T. Liu, *J. Chem. Soc., Faraday Trans. 1*, 83 (1987) 1063.
18. M.R. Gennero De Chialvo, A.C. Chialvo, *Electrochim. Acta,* 33 (1988) 825.
19. C. Bocca, A. Barbucci, G. Cerisola, *Int. J. Hydrogen Energy*, 23 (1998) 247.
20. L.D. Burke, M.E. Lyons, O.J. Murphy, *J. Electroanal. Chem.,* 132 (1982) 247.
21. H. Willems, A.G.C. Kobussen, J.H.W. De Wit, G.H.J. Broers, *J. Electroanal. Chem.,*170 (1984) 227.
22. H. Willems, A.G.C. Kobussen, I.C. Vinke, J.H.W. De Wit, G.H.J. Broers, *J. Electroanal. Chem.,* 194 (1985) 287.
23. M.R. Gennero De Chialvo, A.C. Chialvo, *Electrochim. Acta,* 35 (1990) 437.

24. M.E.G. Lyons, L.D. Burke, *J. Electroanal. Chem.,* 170 (1984) 377.
25. M.E.G. Lyons, M.P. Brandon, *Phys. Chem. Chem. Phys.,* 11 (2009) 2203.
26. R.F. Scarr, *J. Electrochem. Soc.,* 116 (1969) 1526.
27. B.S. Yeo, S.L. Klaus, P.N. Ross, R.A. Mathies, A.T. Bell, *Chem.Phys.Chem,* 11 (2010) 1854.
28. L. D. Burke and E. J. M. O'Sullivan, *J. Electroanal. Chem.,* 117 (1981) 155.
29. L. D. Burke, M. I. Casey, V. J. Cunnane, O. J. Murphy and T. A. M. Twomey, *J. Electroanal. Chem.,* 189 (1985) 353.
30. L. D. Burke and M. E. G. Lyons, *J. Electroanal. Chem.,* 198 (1986) 347.
31. L. D. Burke and D. P.Whelan, *J. Electroanal. Chem.,* 162 (1984) 121.
32. P.G. Pickup, V.I. Birss, *J.Electroanal. Chem*., 220 (1987) 83.
33. S.D. James, *J. Electrochem. Soc.,* 116 (1969) 1681.
34. L.D. Burke, M. McRann, *J. Electroanal. Chem.,* 125 (1981) 387.
35. J.W. Schultze, K.H. Vetter, *Electrochim. Acta,* 18 (1973) 889.
36. W.M. Sachtler, L.L.V. Reizen, *J. Res. Inst. Catal., Hokkaido Univ.,* 10 (1962) 87.
37. R. Woods in *Electroanal. Chem*., Vol. 9, Ed. A.J. Bard, Marcel Dekker, New York, 1976, Ch. 1.
38. L.D.Burke, E.J.M. O'Sullivan, *J. Electroanal. Chem.,* 117 (1981) 155.
39. L.D.Burke, J.K. Mulcahy, *J. Electroanal. Chem.,* 73 (1976) 207.
40. L.D.Burke, M.B.C.Roche, *J. Electroanal. Chem.,* 164 (1984) 315.
41. L.D.Burke, M.M. McCarthy, M.B.C.Roche, *J. Electroanal. Chem*., 167 (1984) 291.
42. M. Gattrell and B. MacDougall, in *Handbook of Fuel Cells- Fundamentals, Technology and Applications*, W. Vielsch, H.A. Gasteiger, A. Lamm (Eds), Vol.2 Electrocatalysis, Chapter 30, pp.443-464, Wiley, (2003).
43. (a) M.E.G. Lyons, M.P. Brandon, *Phys. Chem. Chem. Phys.,* 11 (2009) 2203 ; (b) M.E.G. Lyons, R.L. Doyle, M.P. Brandon, *Analyst,* 2011, submitted for publication.
44. R.A. Robinson and R.H. Stokes, *Electrolyte Solutions*, Revised 2nd Edition, Butterworth & Co. Ltd., London, 1965, p. 492.
45. E.J.M. O'Sullivan, L.D. Burke, *Proc. Symp. Electrocatalysis*, W.E. O'Grady, P.N. Ross, F.G. Will, Eds., Electrochem. Soc., Pennington, NJ, 1982, pp.209-223.
46. E.J.M. O'Sullivan, L.D. Burke, *J. Electrochem. Soc.,* 137 (1990) 466.
47. J.O'M. Bockris and T. Otagawa, *J. Phys. Chem.*, 87 (1983) 2960.
48. (a) B.S. Yeo, S.L. Klaus, P.N. Ross, R.A. Mathies, A.T. Bell, *ChemPhysChem*, 11 (2010) 1854. (b) B.S. Yeo, A.T. Bell, *J. Am. Chem. Soc.,* dx.doi.org/10.1021/ja200559j
49. M.I. Temkin, *Zh. Fiz. Khim.*, 15 (1941) 296.
50. B.E. Conway and E. Gileadi, *Trans. Faraday Soc.*, 58 (1962) 2493.
51. B.E. Conway and E. Gileadi, in *Modern Aspects of Electrochemistry, Vol. 3*, J.O'M. Bockris and B.E. Conway, Eds., Butterworths, London, 1964, p347.
52. M.E.G. Lyons, W. Breen and J.F. Cassidy, *J. Chem. Soc., Faraday Trans.*, 87 (1991) 115.
53. A. Damjanovic, A. Dey and J.O'M. Bockris, *Electrochim. Acta.*, 11 (1966) 791.